LIBS study of ITER relevant tungsten-oxygen coatings exposed to deuterium plasma in Magnum-PSI

I. Jõgi[a], P. Paris[a], M. Laan[a], J. Kozlova[a], H. Mändar[a], M. Passoni[b], D. Dellasega[b], A. Hakola[c], H.J. van der Meiden[d]

[a] *University of Tartu, Institute of Physics, W. Ostwaldi str. 1, 50411 Tartu, Estonia*

[b] *Politecnico di Milano, EURATOM-ENEA-CNR association, Milano, Italy*

[c] *VTT Technical Research Centre of Finland, 02044 VTT, Finland*

[d] *FOM Institute of DIFFER, Dutch Institute for Fundamental Energy Research, 6336 Eindhoven, Netherlands*

Abstract

We discuss the applicability of laser induced breakdown spectroscopy (LIBS) for deuterium retention analysis in compact and porous tungsten-oxide (W-O) coatings. Deuterium loading was performed by exposing the coatings to deuterium plasma in Magnum-PSI linear plasma device.

The deuterium signals obtained by ex-situ LIBS had sufficiently good signal-to-noise ratio for reliable separation of essentially broadened hydrogen and deuterium lines as well as for comparison of the lateral and depth distributions of deuterium in the coatings. Strong deuterium signal was obtained for the first laser shot which corresponded to the surface layer of the W-O coatings whereas deeper in the coating the signal decreased to noise level. In addition, the deuterium signal was highest in the central region of compact W-O coating. For both coatings, depth profiles of elements obtained by LIBS match with those recorded by secondary ion mass spectroscopy (SIMS) in the lateral direction along the sample surface. The results of LIBS and SIMS results were supported by Scanning Electron Microscopy (SEM) and X-ray diffraction (XRD) data which showed that the exposure to deuterium plasma resulted in remarkable changes

in the surface morphology along the sample surface. The study demonstrates the LIBS potential in deuterium retention measurements in plasma facing components.

Keywords: LIBS analysis of ITER relevant tungsten coatings, deuterium loading by Magnum-PSI plasma, diagnostics by SEM, SIMS, XRD

1. Introduction

The retention of fuel (deuterium and tritium) in tungsten (W) is an important research topic in the development of plasma-facing wall components due to the need to keep the tritium inventory in ITER below 700 g [1]. In most of the fuel retention studies, deuterium is used as the proxy for all fusion fuel. The deuterium retention in the plasma-facing components depends both from the plasma parameters and surface properties [2–11]. In fusion reactors the plasma exposure modifies the surfaces by damage and re-deposition of wall material together with fuel and other impurities resulting in the formation of layers with variable porosity, crystallinity and elemental composition [12–17]. Deuterium retention studies with coatings simulating such layers are usually carried out with linear plasma devices. In the case of bulk tungsten used in the plasma-facing components of the reactor divertor, it has been shown that deuterium retention depends on the W grade [3,18,19]. The retention increases considerably for nanocrystalline compact and porous W coatings [6,9]. The presence of other impurity elements, for example oxygen, also influences retention [8,10]. The deuterium retention has shown to increase an order of magnitude in crystalline tungsten-oxide [8] while in porous tungsten-oxide the retention was comparable with bulk tungsten [10]. Such tungsten oxide (W-O) deposits are formed in tokamak divertor tiles during plasma exposure at high temperatures from oxygen contamination originating from vacuum leaks, residual impurities and native oxide in materials [11,14].

Laser induced breakdown spectroscopy (LIBS) has been shown to be a promising method for the in-situ fuel retention monitoring in tokamaks [20–25] and linear plasma devices [26–29]. However, the line intensities in LIBS spectra depend not only on the coating composition but also on morphology and crystalline phase content [30–32]. Besides the spectral lines intensities, the determination of the deuterium retention in the plasma-facing components requires the knowledge of ablation rates of the investigated materials which also depends on the coating

properties [32,33]. These coating properties may be further changed by the exposure of coatings to high plasma fluxes [26,34,35]. This necessitates extensive studies of the influence of coating properties and the parameters of deuterium loading on the LIBS spectra.

The aim of the work was to validate the applicability of LIBS for fuel retention measurements in coatings which have considerably different morphology and crystalline phase content and whose surface was further modified by high deuterium plasma fluxes. For this purpose, the ex-situ LIBS was applied to compact and porous W-O coatings [9,36] which were exposed to high fluence deuterium plasmas in Magnum-PSI. The results of LIBS measurements were related to the deuterium retention and surface properties obtained by secondary ion mass spectroscopy (SIMS), scanning electron microscopy (SEM) and X-ray diffraction (XRD) measurements.

2. Experiment

2.1. Preparation of W-O coatings

The W-O coatings were produced by the pulsed laser deposition (PLD) method from pure metallic W targets in Ar or He atmosphere. The wavelength of the laser beam was 532 nm, the laser fluence 15 J/cm^2 and the distance between target and substrate was 7 cm. More detailed description of other PLD parameters is given in [37,38]. The deposition in He atmosphere at 70 Pa resulted in practically featureless compact coating (Fig. S1a) containing 17 at. % oxygen. The deposition in Ar atmosphere resulted in porous coating (Fig. S1b) with nanostructured features with cauliflower like shape and containing 50 at. % oxygen [36]. The coatings were prepared on stainless steel substrates with the diameter of 30 mm and thickness 1 mm. In the case of porous coating, an adhesion layer of crystalline W was deposited at 10^{-3} Pa [9]. The intended value for coating thickness was approximately 1 μm.

2.2. Deuterium loading by Magnum-PSI plasma

Samples with W-O coatings were exposed to deuterium plasmas of the Magnum-PSI device located in the Dutch Institute DIFFER [39]. The experiments were performed with the new Magnum-PSI setup supplied with superconducting magnet which enabled the use of long

exposure times. The loading was carried out using a 120 A source current during an exposure time of 4050 s. The axial magnetic field of 0.6 T resulted in 20 mm full width at half maximum (FWHM) of the Gaussian plasma beam whereas the full beam diameter was about 35-40 mm. The targets were biased at -40V resulting in an ion energy of about 40 eV. According to the Thomson scattering measurements, the electron temperature was 1.04 eV and electron density $2.5 \cdot 10^{19}$ m^{-3}. These values were used to calculate the ion flux of $1.4 \cdot 10^{23}$ $m^{-2}s^{-1}$. The fluence value determined from the flux and exposure time was $5.7 \cdot 10^{26}$ m^{-2}. The ion flux was chosen as close as possible to ITER relevant fluxes of 10^{24} $m^{-2}s^{-1}$ while keeping the temperature at reasonably low value. Previous studies with tungsten based coatings have used similar fluences with an order of magnitude higher ion flux values comparable to the high fluxes expected in ITER divertor tiles [6,10,40] or orders of magnitude smaller fluences and fluxes [7,9]. The lateral distribution of ion and electron fluxes in linear plasma devices have Gaussian profile whereas the width of the profile is different for ions and electrons. The surface temperature of the samples was 250°C, measured by IR camera. Higher temperature and the use of D and He mixtures would reflect more closely the conditions at ITER walls [34,35] but in present study a relatively low surface temperature was chosen to ensure high deuterium retention [41,42].

2.3. Ex-situ characterization methods

The surface, phase composition and elemental composition analysis methods (SEM, XRD and SIMS) were used to put the LIBS results into perspective i.e. to clarify the properties of coatings on which the LIBS was applied.

The surface and cross-section morphology of coatings at different positions on the surface was determined by high-resolution SEM (HR-SEM) equipped with a focused ion beam (FIB) (Helios^{TM} NanoLab 600 FEI). Elemental distribution along the cross-section of the coatings was determined by energy dispersive X-ray spectroscopy (EDX) using INCA Energy 350 spectrometer (Oxford Instruments). Before the production of the cross-sections of coatings by focused ion beam (FIB), the samples were coated by Pt. The widths of field of view in the obtained images were between 2.56 to 12.8 μm.

XRD analysis by Smartlab (Rigaku) diffractometer was carried out to determine the crystalline phase composition and possible texture of the coatings after deuterium loading. The wavelength of the X-ray radiation was 1.54 Å (Cu Kα line) and the spectra was recorded from 25 to 110°. The instrumental FWHM was 0.25°.

The depth profiles of elements were determined by SIMS and LIBS. LIBS measurements were carried out three weeks after the loading while the time between the loading and SIMS recordings was 5 months. It should be noted that the samples were stored in the plastic bags and the main contamination caused by long storage is the water vapor.

SIMS measurements were made by a double-focusing magnetic sector SIMS (VG IonexIX-70S) with a 5-keV O_2^+ primary ion beam at a current of 250 nA. The analysis area was 0.3x0.4 mm^2 and an electronic gate was used to record the signal from the 10% central region. SIMS measurements were made at different positions along the surface of coatings.

LIBS experiments were carried out with a setup whose detailed description is given in an earlier paper [43]. A pulsed Nd:YAG laser (Quantel) operating at 532 nm and a pulse width of 6 ns was used. The laser beam was focused by a lens with focal length of 150 cm on the sample surface at 90°. The pulse energy was 55 mJ and the corresponding fluence was 25 J/cm^2. The emission of plasma plume was recorded at 45° angle with respect to the laser beam. For the detection of α-lines of hydrogen isotopes, a 0.5 m Czerny-Turner spectrometer coupled with an Andor iStar ICCD camera (DH340T-18F-03) was used to collect the spectrum in ≈ 20 nm wavelength range around 656 nm with a spectral resolution of 0.06 nm (FWHM). An Echelle spectrometer (Andor Technology Mechelle 5000) with an ICCD camera was also used to collect simultaneously the emission spectra in the 250 - 850 nm range. The relative sensitivities of the recording systems were calibrated by deuterium-halogen calibration source (Ocean Optics DH-2000).

The delay between the laser pulse and spectral recording was fixed to 1000 ns and the recording time-gate width was also 1000 ns. The measurements were carried out in an argon atmosphere at 2 Torr. These settings guaranteed optimal separation of the H_α and D_α peaks as well as ensured a good signal-to-noise ratio [43,44]. LIBS measurements were made at different positions along the coating surface and at each position 20 laser shots were applied to obtain depth profiles of the elements.

3. Results and discussion

3.1. Surface of plasma exposed coatings by photographs and SEM

Fig 1 shows photos of compact (upper half) and porous (lower half) samples after the plasma exposure and LIBS testing. The plasma exposure causes the formation of two ring-like patterns, with the central darker one surrounded by a lighter one. Diameters of the dark rings were ≈ 10 and 5 mm for compact and porous coatings, respectively. The width of lighter annular rings was ≈ 5 mm. Similar darker and lighter regions were observed also in previous studies [26,27,45] and their appearance is consistent with the non-uniform distribution of plasma conditions along the coating surface. The surface temperature, plasma temperature and plasma density of Magnum-PSI have Gaussian distribution [26,46]. Furthermore, distributions of electron and ion fluxes of Magnum-PSI are different [46]: the electron flux dominated in the central zone of target (spots 3-7 in compact and spots 5-6 in porous coating) while ion flux dominated in the remaining outer zone.

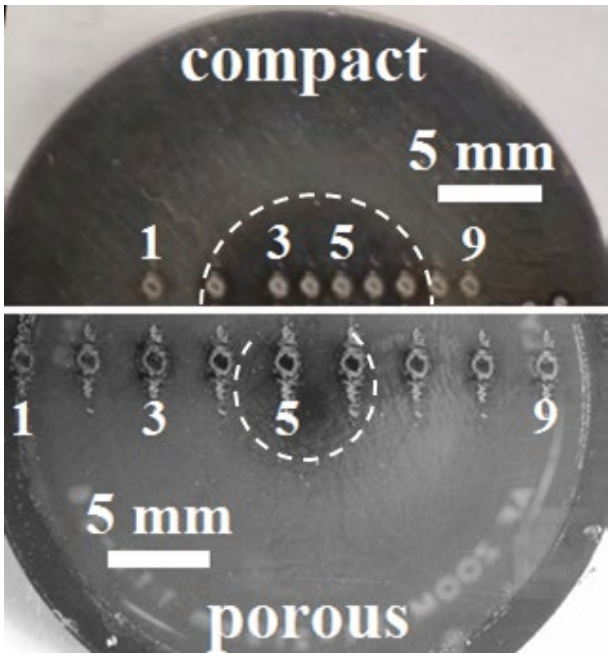

Figure 1. Photographs of upper or lower halves of compact (upper half) and porous (lower half) W-O coating after exposure to deuterium plasma and LIBS measurements. Numbered spots show the positions where LIBS spectra were recorded: each crater was formed by 20 consequent laser pulses. Dashed rings mark the approximate boundary between dark and light regions.

The light region of exposed compact coating had a relatively smooth surface similarly with the unexposed coating (Fig. S1a) but there appeared spots with the size of tens of micrometre where part of the coating was damaged (Fig. 2a). The appearance of these structures can be attributed to the delamination of blisters which are formed due to the accumulation of deuterium inside of the coating [19,47]. In the dark region of compact coating, the spots were missing while there appeared grains of few tens of nanometre size (Fig. 2b). The formation of similar structures was observed also in other studies where fluence values were comparable to that of the present study [6,19,47,48].

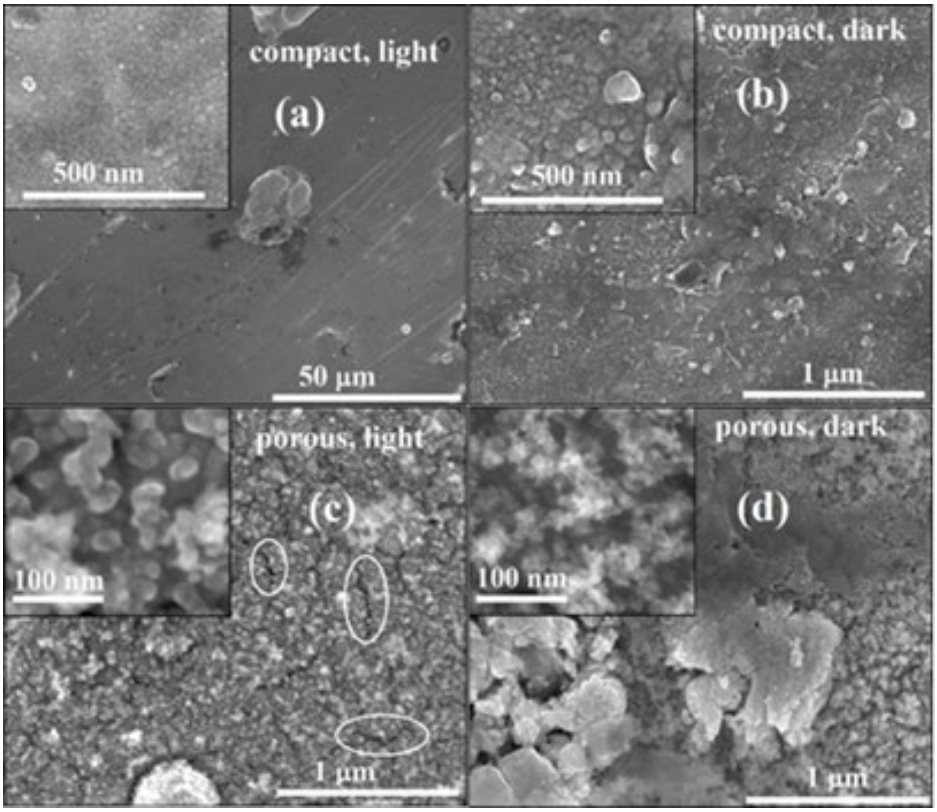

Figure 2. SEM surface images of plasma-exposed compact (a,b) and porous (c,d) W-O coating obtained from light (a,c) and dark (b,d) region. Insets show images with higher magnification. Ovals in (c) mark the positions of cracks.

The light region of the exposed porous coating had nanostructured surface features similarly with unexposed coating (Fig. S1), but plasma exposure caused the appearance of some damage or debris and narrow lengthy cracks (marked by ovals on Fig. 2c). In the dark region of this coating type, the grains were reduced to smaller fuzzy-looking structures (Fig. 2d). In addition,

structureless patterns with the size of hundreds of nanometres could be seen, possibly resulting from re-deposited material on the surface. No signs of coating damage were observed for the porous coating.

3.2. Cross-sections and composition distribution by FIB-SEM and EDX

SEM cross-section images of compact and porous W-O coatings obtained from light and dark regions are shown in figure 3. The surface unevenness of FIB milled cross-sections from the dark region of compact coating is a FIB milling artifact which likely arises because of irregularities on the sample surface as well as due to the variation of the sputtering yield on different crystallographic orientation.

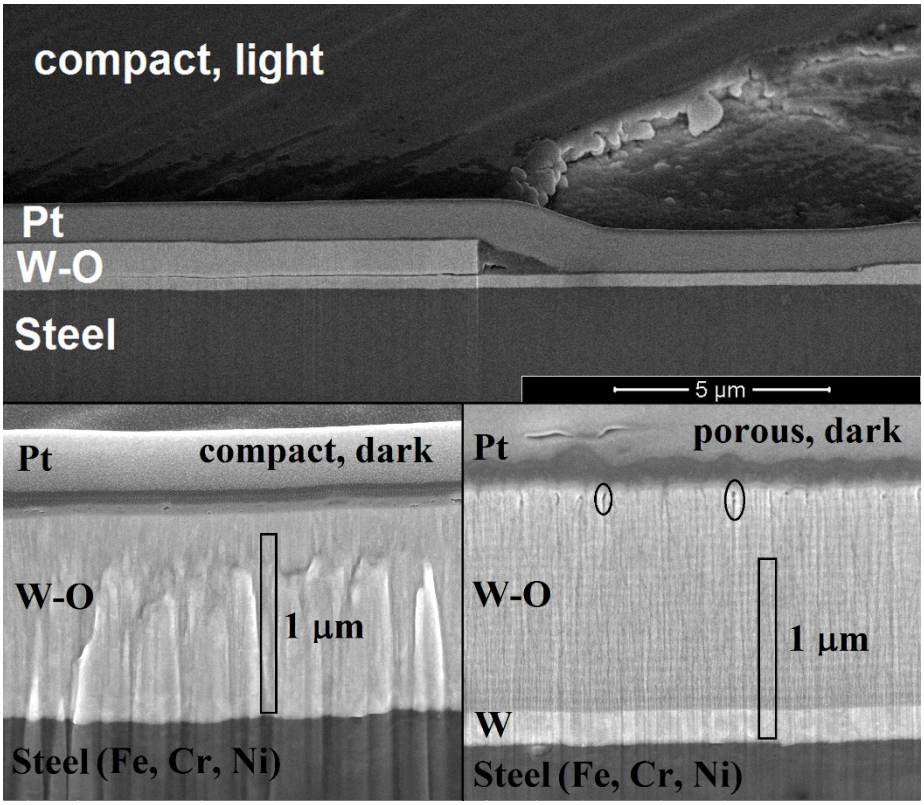

Figure 3. FIB-SEM images of the cross-section of compact and porous W-O coating. The upper panel shows the cross-section of peeled coating, while lower panels show the cross-sections of undamaged coatings from dark regions. The elemental composition of different layers was determined by EDX. Ovals mark the position of cracks.

The cross-section from the light region of a compact W-O coating shows a place where coating damage has taken place. The upper part of the W-O coating in this area was peeled off and the remaining layer of coating was only few hundred nanometers thick. In the dark region, the W-O coating remained undamaged (Fig. 3, lower left panel). In the dark region, above the compact W-O coating was a layer of ≈70 nm thickness. Such distinct surface layer was missing in the light region of compact coating. In both regions the thickness of the unbroken compact W-O coating was between 1.4 to 1.5 μm.

The porous W-O coating remained intact in both regions and the coating thickness was approximately 1.6 μm. The thickness of the W adhesion layer between the steel substrate and the porous W-O coating was approximately 200 nm. The cracks in the porous coating which were apparent from the surface images were also detectable in the cross-section images obtained both from light and dark regions.

3.3. Phase content and crystallite size by XRD

The XRD diffraction patterns of two W-O coatings obtained by theta-2theta scan in the parallel beam configuration are shown in Fig. 4. The most prominent XRD reflections of compact W-O coating can be assigned to 110, 211 and 220 crystallographic planes of the most stable form of tungsten: α-W (ICDD PDF-2 Card 01-089-3012, space group Im-3m). The reflections corresponding to α-W were present in the case of porous W-O coating which had also several weak reflections characteristic to metastable phase of tungsten: β-W (ICDD PDF-2 Card 03-065-6453, crystal structure of A15 type). These reflections were more pronounced in the case of grazing incident configuration which collects signal from the upper layer of surface. For both coatings, there were also small but narrow reflections which corresponded to the steel substrate (marked by S in Fig. 4). It should be noted that the used XRD configuration did not allow to clearly distinguish between light and dark regions, but the signal was expectedly collected mostly from the darker region.

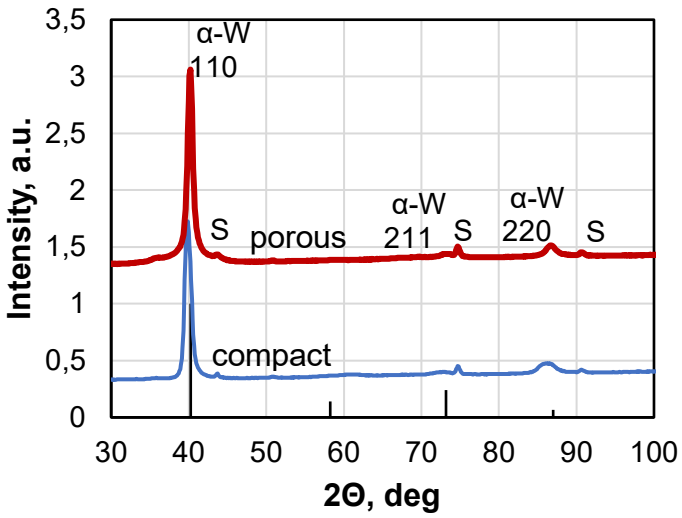

Figure 4. XRD patterns of compact and porous W-O coating obtained by theta-2theta scan.

The intensities and FWHM of reflections were comparable for both coatings. The crystallite size calculated from the FWHM of the dominant reflection (110) of α-W according to Debye-Scherrer formula was about 14 nm for the compact coating and 18 nm for the porous coating. The size of crystallites obtained by XRD is comparable with the grain size of the structures obtained by SEM. Before the exposure to D plasma, the (110) peak of compact coating had considerably lower intensity and broader width when compared to porous coating [36]. The estimated crystallite size was approximately 7 nm for unexposed porous coating and less than 2 nm for unexposed compact coating [36]. The comparison of the results demonstrates considerable increase in the crystallite size of both coatings due to the exposure to the deuterium plasma.

3.4. Elemental depth profiles by SIMS

Depth profiles of deuterium, hydrogen, oxygen, iron and tungsten obtained by SIMS at different regions of compact and porous W-O coatings are shown in figure 5. According to the W profile, the thickness of compact coating was 1.1-1.2 µm and that of the porous coating was 1.5-1.7 µm. These thickness values are close to the values obtained from SEM cross-section images. With the exception of the first 100 nm, the intensity of W signal of all samples did not change remarkably within the thickness of the coating.

Lower W signal at the 100 nm thick surface layer was accompanied with higher Fe signal at the surface. Fe signal diminished inside of the porous coating and dark region of compact coating while the Fe profile in the light region of the compact coating differed drastically from profiles in other characteristic regions. Co-occurrence of strong W and Fe signals in this region seems to indicate that the mixing of these elements could be caused by coating damage (as shown on Fig. 3a) and formation of surface deposits which have mixed nature. Both coating damage and deposits have microscopic size while SIMS integrates over a considerably larger area. It should be noted that the threshold energy for Fe sputtering by deuterium ions is approximately 40 eV [49] which is comparable to the energy of the deuterium ions used in the present study.

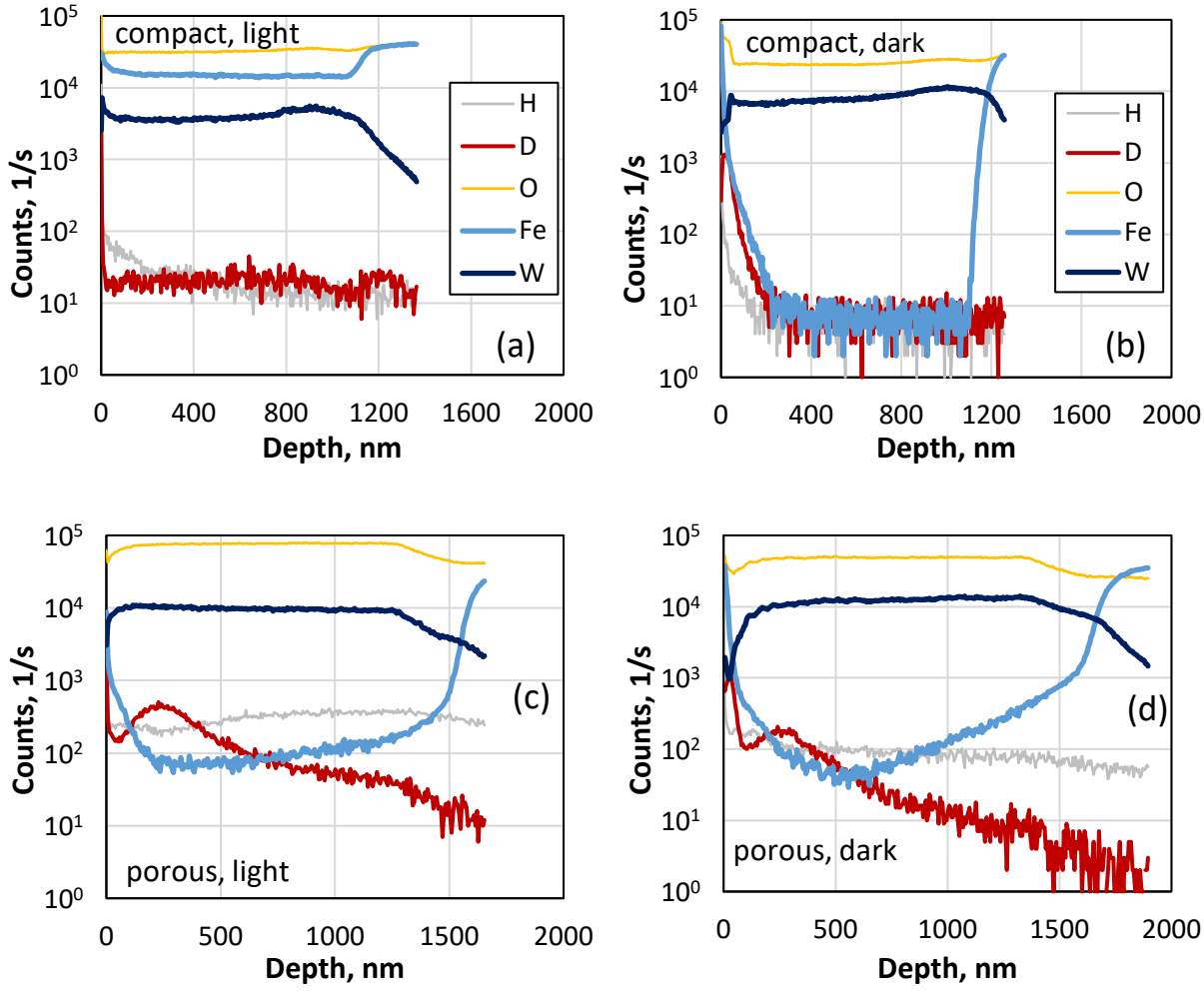

Figure 5. SIMS depth profiles for compact (a,b) and porous (c,d) W-O coating obtained from light (a,c) and dark (b,d) region.

Figures 6a and 6b present the SIMS D signal normalized to W (D/W ratio) which can be used to evaluate the amount of retained D content. For dark regions of both W-O coatings, D/W ratio had peaks in the surface layer of 50 nm thickness whereas somewhat higher peak was obtained for porous W-O coating. Porous W-O coating had an additional hump in the D/W depth profile at the depth of 200-300 nm. This peak was present both in dark and light regions of the coating surface while being somewhat higher in the light region. The presence of the second peak may be caused by D implantation and increased D retention by chemical bonding with oxygen whose concentration is higher in this coating (Fig. 2c and 3). According to earlier study with crystalline tungsten-oxide [8], the bonding with oxygen may be more important than retention in pores. However, the porosity may also influence the retention at higher temperatures and at energies relevant for Magnum-PSI.

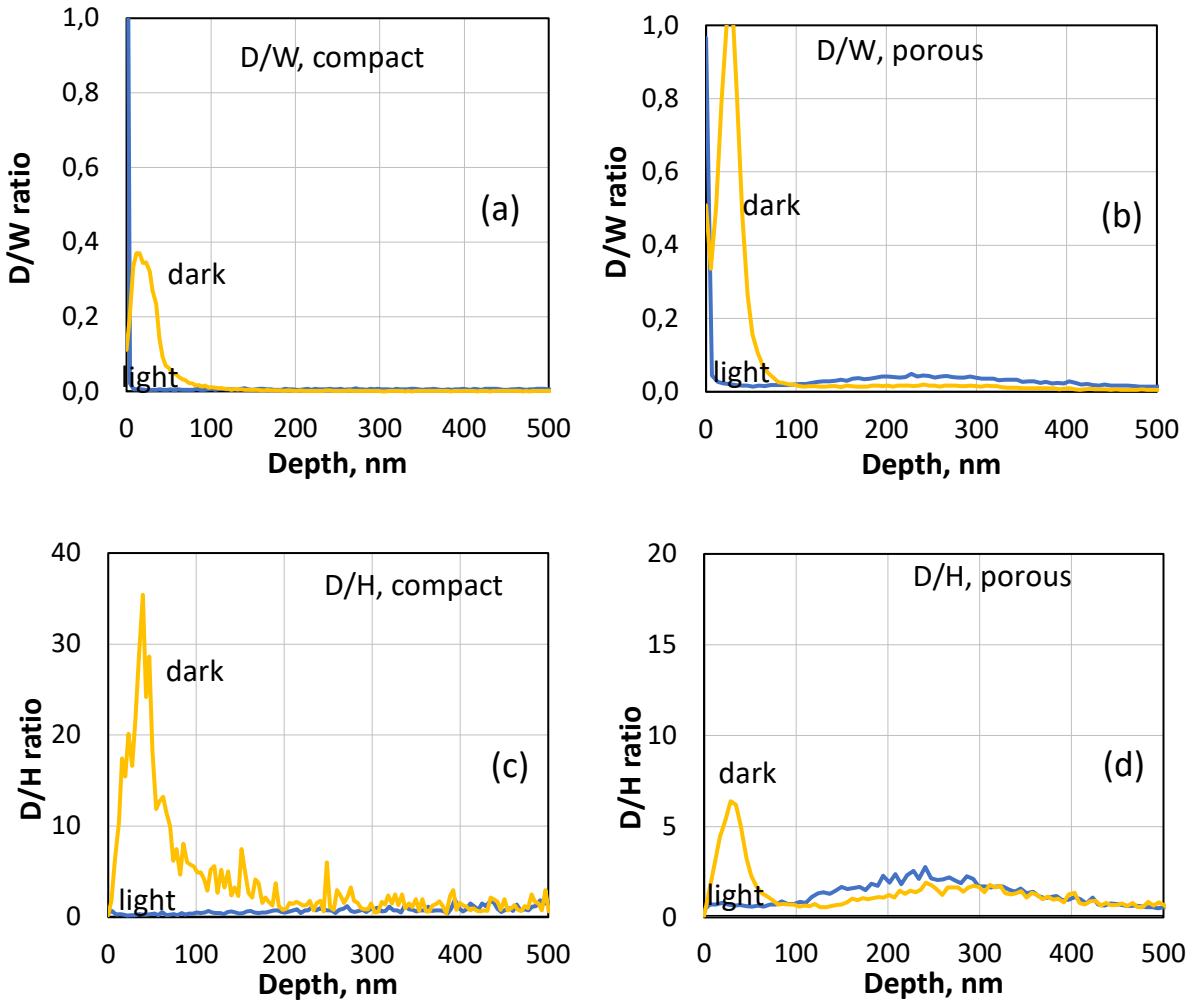

Figure 6. SIMS depth profiles of deuterium signal normalized to tungsten (D/W ratio) (a,b) or hydrogen (D/H ratio) (c,d) obtained from light and dark region of compact (a,c) and porous (b,d) W-O coating.

For further comparison with LIBS results (subsection 3.5), Figures 6c and 6d show the D/H as a function of depth. The general trends in the depth and lateral profiles of D/H ratio are similar to the profiles of D/W ratio, i.e. for both coatings the ratio was largest at the depth less than 100 nm of dark region.

3.5. Elemental depth profiles and deuterium lateral distribution by LIBS

LIBS elemental depth profiles were obtained by applying 20 consecutive laser pulses at the same lateral position. Single shot intensities of the recorded W, Fe and Cr spectral lines had typically poor signal-to noise ratio and depth profiles constructed by different single lines were not unambiguous. To alleviate this problem, several lines of these elements were used for the construction of the depth profiles. At first, the depth profiles of single lines were normalized by the highest intensity of this line. Normalized profiles were then averaged over four W, five Fe and three Cr lines in the wavelength range of 280-520 nm, results are presented in Figure 7.

In the case of the compact coating, the normalized intensity of Fe and Cr lines started to increase after the first shot and reached relatively stable values after 3-4 shots. The intensities of W lines decreased with the growth of Fe and Cr line intensities but were even noisier. It should be noted that the coating-substrate interface of LIBS depth profiles is smeared because the substrate is reached faster at the center of the laser beam due to its Gaussian profile of the intensity. Therefore the resulting LIBS spectra will contain emission lines simultaneously from the substrate and from the sides of the coating [50]. The compact coating was removed by very small number of shots and the resulting small depth resolution did not allow a more detailed comparison of LIBS and SIMS results for compact coating. The LIBS elemental depth profiles of porous coating followed the trends in SIMS depth profiles. The normalized intensity of Fe and Cr lines started to grow from shot 3-4 onwards reaching stable values after 5-6 shots.

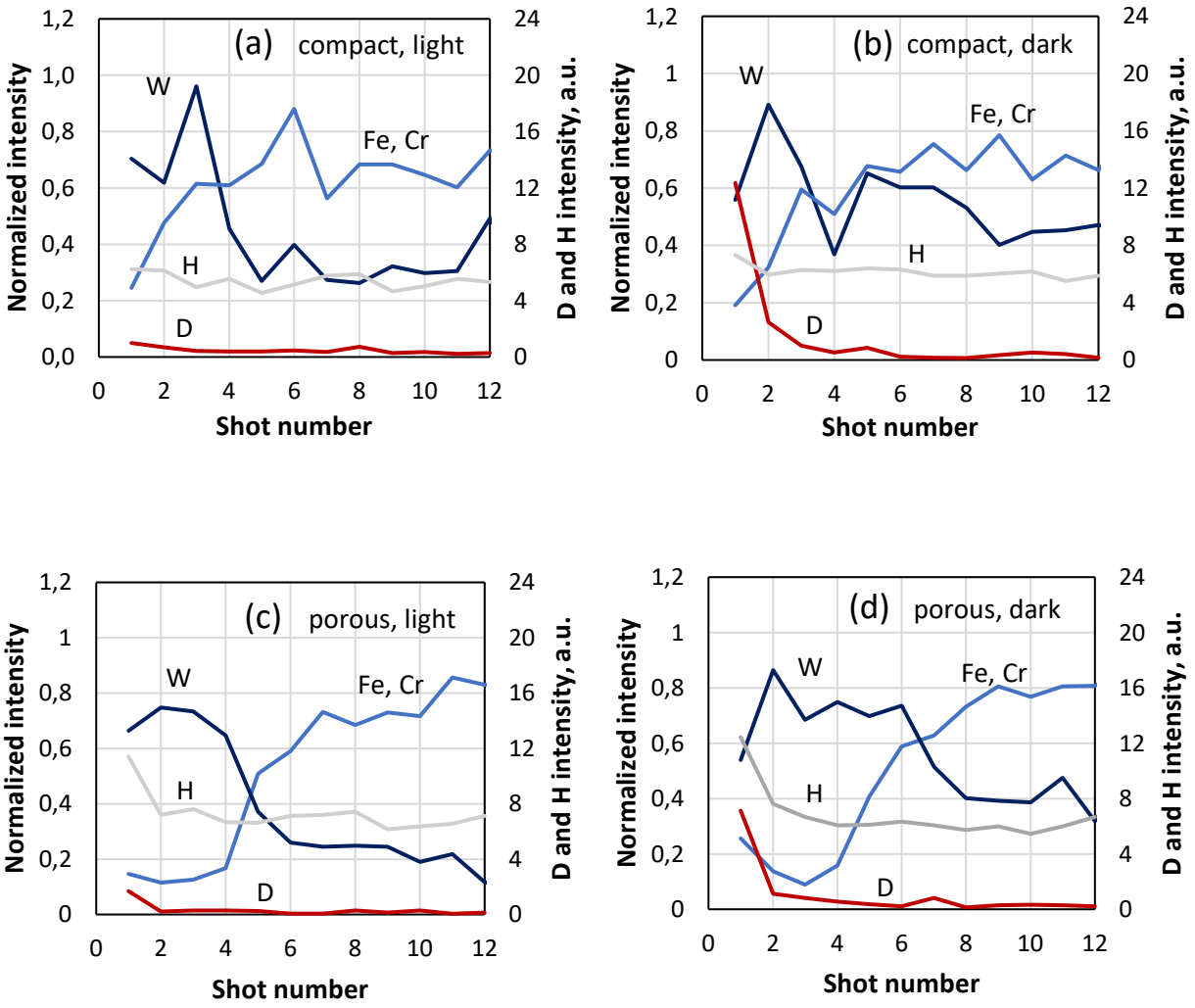

Figure 7. LIBS depth profiles for the averaged intensity of normalized W, Fe and Cr lines and intensity of D_α and H_α lines for compact (a,b) and porous (b,c) W-O coatings obtained from light (a,c) and dark (b,d) regions of the coating.

The ablation rate of the coatings was estimated from the thickness of the coating and the number of laser shots required to remove the coating. It should be noted that this calculation procedure gives an average value over a number of shots while the ablation rates of single shots may vary due to the changing crater size [50] and coating properties [32]. The ablation rate of the compact W-O coating estimated by the described procedure was 350-460 nm/shot. Large uncertainty in the ablation rate of this coating is mainly caused by the small number of shots required to reach the substrate. Ablation rate of porous coating calculated in a similar way was 250-300 nm/shot.

The calculated rate is probably influenced by the presence of 200 nm thick crystalline W interlayer between the porous coating and substrate. This dense interlayer may have ablation rate even below 100 nm/shot according to our earlier studies which investigated the ablation rates of various W coatings [32].

Figure 8 shows the LIBS spectra in the wavelength region around 656 nm which were obtained by subsequent laser shots at spot 5 (Fig. 1) in the dark region of the compact coating. The spectra of the first shots had two peaks at 656.1 and 656.28 nm corresponding to partly overlapped D_α and H_α lines. The intensities of these lines were obtained by fitting with Lorentzian contours (FWHM value 0.16 nm). According to figure 8, the use of Lorentzian contours resulted in good fit of the experimentally determined peaks. For all spots the intensity of the H_α line, I_H, slightly decreased after the first shot and then remained almost unchanged for subsequent laser shots while for the second shot the D_α intensity was at least five time less than it was for the first shot (Fig. 7a). For measured spots of the light region of the compact coating, the D_α intensity exceeds the noise level only for the first shot while H_α line intensities followed the intensities determined in dark region (Fig. 7). In case of the porous coating, the D_α line was observable only for the first shot regardless of the region on the surface. H_α line intensities of porous coating was almost the same as in the case of compact coating (Fig. 7). Furthermore, for both coatings the intensity of H_α line remained practically unchanged in W-O coating and steel substrate.

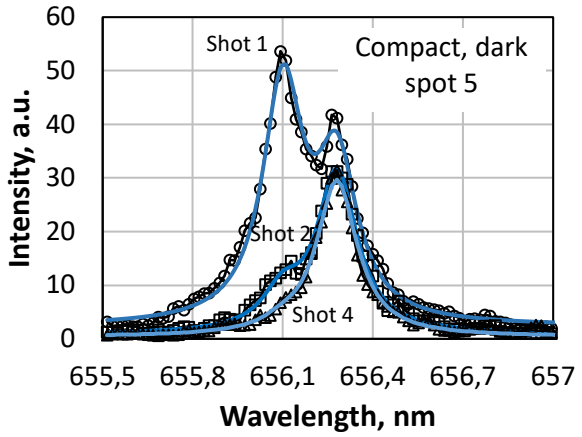

Figure 8. LIBS recordings of deuterium and hydrogen lines obtained by subsequent laser shots from the dark region of compact W-O coating at spot 5 shown on figure 1. Dots represent the experimental values and solid lines the Lorentzian fit.

Figure 9 shows spectra of hydrogen isotopes of the first shot obtained from different spots on compact and porous coatings. In the case of compact coatings, the intensity of the H_α line remained practically constant along the surface while the intensity of the D_α line decreased gradually with the distance from the center. In the case of the porous coating, the intensity of the H_α line was comparable with the intensity of the H_α line obtained for compact coatings but the D_α intensity had no clear correlation with the position on the coating.

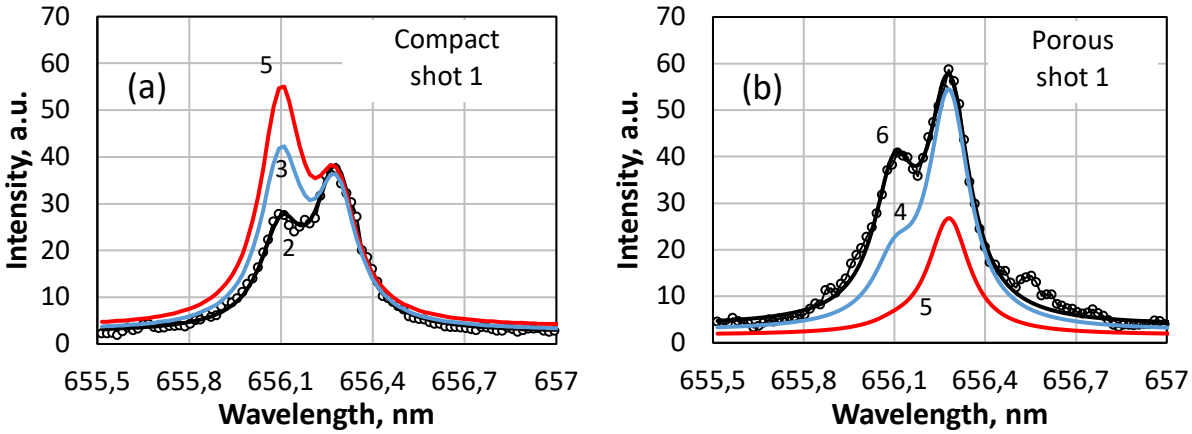

Figure 9. LIBS recordings of deuterium and hydrogen lines obtained by the first laser shot from the (a) compact and (b) porous W-O coating at different regions on the surface. The spot locations are shown by numbers in figure 1. Dots represent the experimental values and solid lines are Lorentzian fits.

In the case of SIMS data, the use of D/W and D/H ratios allowed a better presentation of the regularities of D retention. In the case of LIBS only the I_D/I_H ratio gave reliable results as the I_W signal was weak and noisy. Average intensity of H_α line from shots 2-12 with nearly constant H intensity (Fig. 7) was used for normalization. The I_D/I_H lateral profiles of compact and porous coatings are shown in Fig. 10. The lateral profile obtained for compact coating was fitted by a Gaussian profile because the deuterium plasma beam had also Gaussian profile. However, the FWHM of plasma beam was 20 mm while the FWHM of the deuterium distribution profile was ≈ 10 mm, comparable to the width of the dark region of this coating. The results suggest that

deuterium distribution profile in compact coating might be caused by the differences in ion and electron fluxes similarly with the width of the dark region (section 3.1). At the same time, the ratio I_D/I_H of porous coatings had no clear correlation with the position on the surface of coating.

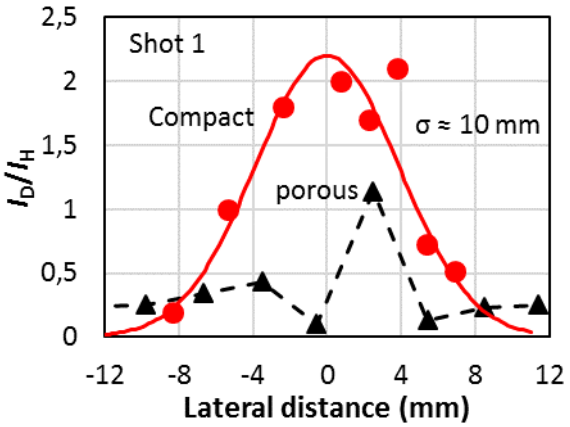

Figure 10. Lateral profile of deuterium relative intensity I_D/I_H for compact and porous coatings. The distance was given from the center of the dark region. The lateral profile corresponding to compact coating was fitted by gaussian shown as red line.

The LIBS lateral and depth profiles of deuterium relative intensities are generally in line with the D/H ratios obtained by SIMS results (Fig. 6c and 6d) and show that considerable amount of deuterium was loaded only in the thin surface layer of dark region of the W-O coatings.

4. Summary/Conclusions

We have investigated the possibility to use LIBS for the determination of deuterium retention in tungsten-oxide coatings with markedly different properties. The samples were exposed to deuterium plasma flux which was chosen as close as possible to ITER relevant value while the surface temperature of samples was kept low to ensure high deuterium retention. The exposure to plasma caused the appearance of central and peripheral zones at the surface of samples whose surface morphology and elemental composition differed markedly.

- According to FIB-SEM pictures, in the case of compact coating the peeling of the coating takes place in the peripheral zone and as a result in SIMS depth profiles intensive signals of the substrate material arises at all depth values. Large fluctuations of the LIBS W and

Fe/Cr signals permitted just a rough estimation of the ablation rate. In addition, these fluctuations did not allow to use the ratio I_D/I_W for comparison of LIBS and SIMS results. However, it appeared that in LIBS measurements the intensity of H_α line depended only a little on the laser shot number. This circumstance gave a possibility to compare results of deuterium retention obtained by LIBS and SIMS. Both LIBS and SIMS measurements showed that the ratio of deuterium to hydrogen was highest in the central region of plasma treated compact coating. Strong deuterium signals of LIBS during the first laser shot matches with the SIMS finding that the deuterium was accumulated only in the narrow region near the coating surface.

- For porous coating FIB-SEM pictures did not show the coating peeling and the LIBS and SIMS gave qualitatively similar W and Fe depth profiles with relatively uniform depth distribution of W along the coating. Deuterium was detectable only during the first LIBS shots while the spatial distribution of the LIBS ratio of deuterium to hydrogen had no clear correlation with the regions on the surface of porous coating.

Final remarks concern the planning of further studies. First, the described results of ex-situ measurements do not reflect the actual on-line retention because of deuterium outgassing. The initial retention immediately after the deuterium plasma exposure can be found carrying out LIBS measurements immediately after exposure to plasma. Secondly, the quantitative estimation of the fuel retention becomes possible when instead of H_α line, the lines of an element with known concentration are used.

Acknowledgements

This work has been carried out within the framework of the EUROfusion Consortium and has received funding from the Euratom research and training programme 2014-2018 and 2019-2020 under grant agreement number 633053. The views and opinions expressed herein do not necessarily reflect those of the European Commission. We are grateful for the aid of Magnum Contributors.

References

[1] J. Roth, E. Tsitrone, T. Loarer, V. Philipps, S. Brezinsek, A. Loarte, G.F. Counsell, R.P. Doerner, K. Schmid, O.V. Ogorodnikova, R.A. Causey, Tritium inventory in ITER plasma-facing materials and tritium removal procedures, Plasma Phys. Control. Fusion. 50 (2008) 103001.

[2] L. Buzi, G. De Temmerman, B. Unterberg, M. Reinhart, A. Litnovsky, V. Philipps, G. Van Oost, S. Möller, Influence of particle flux density and temperature on surface modifications of tungsten and deuterium retention, J. Nucl. Mater. 455 (2014) 316–319. doi:10.1016/j.jnucmat.2014.06.059.

[3] L. Buzi, G. De Temmerman, B. Unterberg, M. Reinhart, T. Dittmar, D. Matveev, C. Linsmeier, U. Breuer, A. Kreter, G. Van Oost, Influence of tungsten microstructure and ion flux on deuterium plasma-induced surface modifications and deuterium retention, J. Nucl. Mater. 463 (2015) 320–324. doi:10.1016/j.jnucmat.2014.12.006.

[4] Y.Z. Jia, G. De Temmerman, G.N. Luo, H.Y. Xu, C. Li, B.Q. Fu, W. Liu, Surface morphology and deuterium retention in tungsten exposed to high flux D plasma at high temperatures, J. Nucl. Mater. 457 (2015) 213–219. doi:10.1016/j.jnucmat.2014.11.079.

[5] A. Kreter, D. Nishijima, R.P. Doerner, M. Freisinger, C. Linsmeier, Y. Martynova, S. Möller, M. Rasinski, M. Reinhart, A. Terra, Y. Torikai, B. Unterberg, Influence of plasma impurities on the fuel retention in tungsten, Nucl. Fusion. 59 (2019). doi:10.1088/1741-4326/ab235d.

[6] M.H.J. Hoen, D. Dellasega, A. Pezzoli, M. Passoni, A.W. Kleyn, P.A.Z. Emmichoven, Deuterium retention and surface modifications of nanocrystalline tungsten films exposed to high-flux plasma, J. Nucl. Mater. 463 (2015) 989–992.

[7] O. V. Ogorodnikova, Effect of nanostructure on radiation tolerance and deuterium retention in tungsten, J. Appl. Phys. 122 (2017). doi:10.1063/1.4996096.

[8] V.K. Alimov, B. Tyburska, M. Balden, S. Lindig, J. Roth, K. Isobe, T. Yamanishi, Surface morphology and deuterium retention in tungsten oxide layers exposed to low-energy, high flux D plasma, J. Nucl. Mater. 409 (2011) 27–32.

[9] O.V. Ogorodnikova, C. Ruset, D. Dellasega, A. Pezzoli, M. Passoni, K. Sugiyama, Y. Gasparayan, V. Efimov, Deuterium retention in dense and disordered nanostructured tungsten coatings, J. Nucl. Mater. 507 (2018) 226–240.

[10] A. Pezzoli, D. Dellasega, V. Russo, A. Gallo, P.A.. Zeijlmans van Emmichoven, M. Passoni, E. Besozzi, D. Dellasega, V. Russo, C. Conti, M. Passoni, M.G. Beghi, A. Maffini, A. Uccello, D. Dellasega, M. Passoni, Thermal annealing and exposure to divertor-like deuterium plasma of

tailored tungsten oxide coatings, J. Nucl. Mater. 463 (2015) 1041–1044. doi:10.1016/j.matdes.2018.107565.

[11] A. Litnovsky, M. Matveeva, A. Herrmann, V. Rohde, M. Mayer, K. Sugiyama, K. Krieger, V. Voitsenya, G. Vayakis, A.E. Costley, R. Reichle, G. De Temmerman, S. Richter, U. Breuer, L. Buzi, S. Möller, V. Philipps, U. Samm, P. Wienhold, First studies of ITER-diagnostic mirrors in a tokamak with an all-metal interior: Results of the first mirror test in ASDEX Upgrade, Nucl. Fusion. 53 (2013). doi:10.1088/0029-5515/53/7/073033.

[12] M. Mayer, J. Likonen, J.P. Coad, H. Maier, M. Balden, S. Lindig, E. Vainonen-Ahlgren, V. Philipps, Tungsten erosion in the outer divertor of JET, J. Nucl. Mater. 363–365 (2007) 101–106. doi:10.1016/j.jnucmat.2007.01.010.

[13] M. Mayer, M. Andrzejczuk, R. Dux, E. Fortuna-Zalesna, A. Hakola, S. Koivuranta, K. Krieger, K.J. Kurzydlowski, J. Likonen, G. Matern, R. Neu, G. Ramos, M. Rasinski, V. Rohde, K. Sugiyama, A. Wiltner, W. Zielinski, Tungsten erosion and redeposition in the all-tungsten divertor of ASDEX Upgrade, Phys. Scr. T. T138 (2009). doi:10.1088/0031-8949/2009/T138/014039.

[14] M. Rasinski, E. Fortuna-Zalesna, M. Mayer, R. Neu, T. Plocinski, M. Lewandowska, K.J. Kurzydlowski, High resolution scanning transmission electron microscopy (HR STEM) analysis of re-deposited layer on ASDEX Upgrade tile, Fusion Eng. Des. 86 (2011) 1753–1756. doi:10.1016/j.fusengdes.2011.02.085.

[15] A. Kallenbach, M. Balden, R. Dux, T. Eich, C. Giroud, A. Huber, G.P. Maddison, M. Mayer, K. McCormick, R. Neu, T.W. Petrie, T. Pütterich, J. Rapp, M.L. Reinke, K. Schmid, J. Schweinzer, S. Wolfe, Plasma surface interactions in impurity seeded plasmas, J. Nucl. Mater. 415 (2011) S19–S26. doi:10.1016/j.jnucmat.2010.11.105.

[16] J. Likonen, E. Alves, A. Baron-Wiechec, S. Brezinsek, J.P. Coad, A. Hakola, K. Heinola, S. Koivuranta, G.F. Matthews, P. Petersson, M. Rubel, C. Stan-Sion, A. Widdowson, First results and surface analysis strategy for plasma-facing components after JET operation with the ITER-like wall, Phys. Scr. T159 (2014) 014016. doi:10.1088/0031-8949/2014/t159/014016.

[17] E. Fortuna-Zalesna, M. Andrzejczuk, L. Ciupinski, K. Rozniatowski, K. Sugiyama, M. Mayer, K.J. Kurzydlowski, Post mortem analysis of a tungsten coated tile from the outer divertor strike point region of ASDEX upgrade, Nucl. Mater. Energy. 9 (2016) 128–131. doi:10.1016/j.nme.2016.10.011.

[18] K. Sugiyama, M. Mayer, A. Herrmann, K. Krieger, V. Rohde, M. Balden, S. Lindig, R. Neu, H.W.

Müller, Deuterium retention in tungsten used in ASDEX Upgrade: Comparison of tokamak and laboratory studies, Phys. Scr. T159 (2014). doi:10.1088/0031-8949/2014/T159/014043.

[19] M. Balden, A. Manhard, S. Elgeti, Deuterium retention and morphological modifications of the surface in five grades of tungsten after deuterium plasma exposure, J. Nucl. Mater. 452 (2014) 248–256. doi:10.1016/j.jnucmat.2014.05.018.

[20] V. Philipps, A. Malaquias, A. Hakola, J. Karhunen, G. Maddaluno, S. Almaviva, L. Caneve, F. Colao, E. Fortuna, P. Gasior, M. Kubkowska, A. Czarnecka, M. Laan, A. Lissovski, P. Paris, H.J. van der Meiden, P. Petersson, M. Rubel, A. Huber, M. Zlobinski, B. Schweer, N. Gierse, Q. Xiao, G. Sergienko, Development of laser-based techniques for in situ characterization of the first wall in ITER and future fusion devices, Nucl. Fusion. 53 (2013) 093002. doi:10.1088/0029-5515/53/9/093002.

[21] A. Semerok, D. L'Hermite, J.-M. Weulersse, J.-L. Lacour, G. Cheymol, M. Kempenaars, N. Bekris, C. Grisolia, Laser induced breakdown spectroscopy application in joint European torus, Spectrochim. Acta Part B. 123 (2016) 121–128.

[22] D. Zhao, C. Li, Z. Hu, C. Feng, Q. Xiao, R. Hai, P. Liu, L. Sun, D. Wu, C. Fu, J. Liu, N. Farid, F. Ding, G.-N. Luo, L. Wang, H. Ding, Remote in situ laser-induced breakdown spectroscopic approach for diagnostics of the plasma facing components on experimental advanced superconducting tokamak, Rev. Sci. Instrum. 89 (2018) 073501.

[23] G. Maddaluno, S. Almaviva, L. Caneve, F. Colao, V. Lazic, L. Laguardia, P. Gasior, M. Kubkowska, Detection by LIBS of the deuterium retained in the FTU toroidal limiter, Nucl. Mater. Energy. 18 (2019) 208–211. doi:10.1016/j.nme.2018.12.029.

[24] S. Almaviva, L. Caneve, F. Colao, V. Lazic, G. Maddaluno, P. Mosetti, A. Palucci, A. Reale, P. Gasior, W. Gromelski, M. Kubkowska, LIBS measurements inside the FTU vessel mock-up by using a robotic arm, Fusion Eng. Des. 157 (2020) 111685. doi:10.1016/j.fusengdes.2020.111685.

[25] C. Li, L. Sun, Z. Hu, D. Zhao, J. Liu, N. Gierse, D. Nicolai, D. Wu, R. Hai, F. Ding, G.N. Luo, S. Brezinsek, C. Linsmeier, Y. Liang, H. Ding, An in situ diagnostic method for monitoring of fuel retention on the first wall under long-pulse operation of experimental advanced superconducting tokamak, Phys. Scr. 2020 (2020). doi:10.1088/1402-4896/ab6005.

[26] K. Piip, H.J. van der Meiden, L. Hämarik, J. Karhunen, A. Hakola, M. Laan, P. Paris, M. Aints, J. Likonen, K. Bystrov, J. Kozlova, A. Založnik, M. Kelemen, S. Markelj, LIBS detection of erosion/deposition and deuterium retention resulting from exposure to Pilot-PSI plasmas, J. Nucl.

Mater. 489 (2017) 129–136. doi:10.1016/j.jnucmat.2017.03.044.

[27] K. Piip, H.J. van der Meiden, K. Bystrov, L. Hämarik, J. Karhunen, M. Aints, M. Laan, P. Paris, H. Seemen, A. Hakola, S. Brezinsek, Loading of deuterium and helium by Pilot-PSI plasma and their detection by in-situ LIBS, Nucl. Mater. Energy. 12 (2017) 694–698. doi:10.1016/j.nme.2016.12.034.

[28] X. Jiang, G. Sergienko, B. Schweer, N. Gierse, M. Hubeny, A. Kreter, S. Brezinsek, Design and development of a LIBS system on linear plasma device PSI-2 for in situ real-time diagnostics of plasma-facing materials, Nucl. Mater. Energy. 12 (2017) 1224–1230.

[29] D. Nishijima, M. Patino, R.P. Doerner, Development of a LIBS system for in situ surface measurements during plasma exposure in PISCES-A, Rev. Sci. Instrum. 89 (2018) 10J105.

[30] N.B. Zorov, A.A. Gorbatenko, T.A. Labutin, A.M. Popov, A review of normalization techniques in analytical atomic spectrometry with laser sampling: From single to multivariate correction, Spectrochim. Acta - Part B At. Spectrosc. 65 (2010) 642–657. doi:10.1016/j.sab.2010.04.009.

[31] E. Tognoni, G. Cristoforetti, Signal and noise in Laser Induced Breakdown Spectroscopy: An introductory review, Opt. Laser Technol. 79 (2016) 164–172. doi:10.1016/j.optlastec.2015.12.010.

[32] M. Laan, A. Hakola, P. Paris, K. Piip, M. Aints, I. Jõgi, J. Kozlova, H. Mändar, C. Lungu, C. Porosnicu, E. Grigore, C. Ruset, J. Kolehmainen, S. Tervakangas, Dependence of LIBS spectra on the surface composition and morphology of W/Al coatings, Fusion Eng. Des. 121 (2017). doi:10.1016/j.fusengdes.2017.03.173.

[33] J. Karhunen, A. Hakola, J. Likonen, A. Lissovski, M. Laan, P. Paris, Applicability of LIBS for in situ monitoring of deposition and retention on the ITER-like wall of JET - Comparison to SIMS, J. Nucl. Mater. 463 (2015) 931–935. doi:10.1016/j.jnucmat.2014.10.028.

[34] S. Gonderman, J.K. Tripathi, T.J. Novakowski, T. Sizyuk, A. Hassanein, Effect of dual ion beam irradiation (helium and deuterium) on tungsten–tantalum alloys under fusion relevant conditions, Nucl. Mater. Energy. 12 (2017) 346–352. doi:10.1016/j.nme.2017.02.011.

[35] T.J. Novakowski, A. Sundaram, J.K. Tripathi, S. Gonderman, A. Hassanein, Deuterium desorption from ion-irradiated tantalum and effects on surface morphology, J. Nucl. Mater. 504 (2018) 1–7. doi:10.1016/j.jnucmat.2018.03.023.

[36] R. Mateus, D. Dellasega, M. Passoni, Z. Siketić, I. Bogdanović Radović, A. Hakola, E. Alves, Helium load on W-O coatings grown by pulsed laser deposition, Surf. Coatings Technol. 355

(2018) 215–221. doi:10.1016/j.surfcoat.2018.02.089.

[37] D. Dellasega, G. Merlo, C. Conti, C.E. Bottani, M. Passoni, Nanostructured and amorphous-like tungsten films grown by pulsed laser deposition, J. Appl. Phys. 112 (2012) 084328. doi:10.1063/1.4761842.

[38] A. Maffini, A. Uccello, D. Dellasega, M. Passoni, Laser cleaning of diagnostic mirrors from tungsten-oxygen tokamak-like contaminants, Nucl. Fusion. 56 (2016). doi:10.1088/0029-5515/56/8/086008.

[39] H.J.N. Van Eck, A.W. Kleyn, A. Lof, H.J. Van Der Meiden, G.J. Van Rooij, J. Scholten, P.A. Zeijlmans Van Emmichoven, Divertor conditions relevant for fusion reactors achieved with linear plasma generator, Appl. Phys. Lett. 101 (2012). doi:10.1063/1.4768302.

[40] E. Vassallo, R. Caniello, G. Angella, D. Dellasega, G. Granucci, V. Mellera, D. Minelli, M. Pedroni, D. Ricci, V. Rigato, M. Passoni, Retention of nanocrystalline WN<inf>x</inf> layers exposed to high-fluence deuterium plasmas, J. Nucl. Mater. 466 (2015) 621–626. doi:10.1016/j.jnucmat.2015.09.006.

[41] J. Roth, K. Schmid, Hydrogen in tungsten as plasma-facing material, Phys. Scr. T. T145 (2011). doi:10.1088/0031-8949/2011/T145/014031.

[42] W.R. Wampler, Temperature dependence of deuterium retention mechanisms in tungsten, Phys. Scr. T171 (2020) 014012.

[43] P. Paris, J. Butikova, M. Laan, M. Aints, A. Hakola, K. Piip, I. Tufail, P. Veis, Detection of deuterium retention by LIBS at different background pressures, Phys. Scr. T170 (2017) 014003.

[44] L. Mercadier, J. Hermann, C. Grisolia, A. Semerok, Plume segregation observed in hydrogen and deuterium containing plasmas produced by laser ablation of carbon fiber tiles from a fusion reactor, Spectrochim. Acta - Part B At. Spectrosc. 65 (2010) 715–720. doi:10.1016/j.sab.2010.04.011.

[45] K. Piip, G. De Temmerman, H.J. Van Der Meiden, A. Lissovski, J. Karhunen, M. Aints, A. Hakola, P. Paris, M. Laan, J. Likonen, I. Jõgi, J. Kozlova, H. Mändar, LIBS analysis of tungsten coatings exposed to Magnum PSI ELM-like plasma, J. Nucl. Mater. 463 (2015). doi:10.1016/j.jnucmat.2014.11.017.

[46] C. Costin, V. Anita, G. Popa, J. Scholten, G. De Temmerman, Tailoring the charged particle fluxes across the target surface of Magnum-PSI, Plasma Sources Sci. Technol. 25 (2016).

doi:10.1088/0963-0252/25/2/025023.

[47] W. Guo, L. Cheng, J. Wang, Q. Fu, S. Qin, Y. Yuan, G.H. Lu, Nanostructure evolution and surface modification of tungsten exposed to low energy, high flux deuterium plasma, Fusion Eng. Des. 125 (2017) 473–478. doi:10.1016/j.fusengdes.2017.04.057.

[48] M.H.J. 'T Hoen, M. Balden, A. Manhard, M. Mayer, S. Elgeti, A.W. Kleyn, P.A. Zeijlmans Van Emmichoven, Surface morphology and deuterium retention of tungsten after low- and high-flux deuterium plasma exposure, Nucl. Fusion. 54 (2014). doi:10.1088/0029-5515/54/8/083014.

[49] K. Sugiyama, K. Schmid, W. Jacob, Sputtering of iron, chromium and tungsten by energetic deuterium ion bombardment, Nucl. Mater. Energy. 8 (2016) 1–7. doi:10.1016/j.nme.2016.05.016.

[50] G. Shaw, M. Bannister, T.M. Biewer, M.Z. Martin, F. Meyer, B.D. Wirth, The detection of He in tungsten following ion implantation by laser-induced breakdown spectroscopy, Appl. Surf. Sci. 427 (2018) 695–703. doi:10.1016/j.apsusc.2017.08.180.